CHEMISTRY
A EUROPEAN JOURNAL

DOI: 10.1002/chem.200903290

Molecular Structure of Amyloid Fibrils Formed by Residues 127 to 147 of the Human Prion Protein

Ni-Shian Lin,[a] John Ching-Hao Chao,[a] Hsin-Mei Cheng,[a] Fang-Chieh Chou,[a] Chi-Fon Chang,[b] Yun-Ru Chen,[b] Yu-Jen Chang,[b] Shing-Jong Huang,[a] and Jerry C. C. Chan*[a]

Abstract: Amyloid fibrils are filamentous and insoluble forms of peptides or proteins. Proline has long been considered to be incompatible with the cross-β structural motif of amyloid fibrils. On the basis of solid-state NMR spectroscopy data, we present a structural model of an in-register parallel β sheet for the amyloid fibrils formed from a human prion protein fragment, huPrP$_{127–47}$. We have developed a simple solid-state NMR spectroscopy technique to identify solvent-protected backbone amide protons in a H/D exchange experiment without disaggregating the amyloid fibrils, from which we find that proline residue P_{137} does not disrupt the β-sheet structure from G_{127} to G_{142}. We suggest that the resultant kink at P_{137} generates a twist between adjacent peptide strands to maintain hydrogen bonding in the β-sheet regions flanking the P_{137} residue. Although proline can be well integrated into the cross-β structure of amyloid fibrils, the kink formed at the position of the proline residue will considerably weaken the hydrogen bonding between the neighboring strands, especially when the mutation site is near the central region of a β sheet.

Keywords: amyloid beta-peptides · H/D exchange · NMR spectroscopy · proline · protein structures

Introduction

Amyloid fibrils are filamentous and insoluble forms of peptides or proteins. Research studies of amyloid fibrils are being actively pursued because of their occurrence in neurodegenerative diseases, such as Alzheimer's disease, type II diabetes, Huntington's disease, and prion diseases.[1] It has been known for some years that the amyloid fibrils formed by peptide sequences with very different biophysical properties have many structural features in common.[2] To unravel the physical principles governing this interesting phenomenon, which can provide significant mechanistic insights into the self-assembly of macromolecules, it is necessary to determine the molecular structures of amyloid fibrils formed by a large variety of proteins or their fragments.[3] In this regard, amyloidogenic sequences containing proline are particularly interesting because it has been reported that proline has a strong propensity to suppress amyloid formation.[4] On the basis of this finding, scanning proline mutagenesis experiments have been employed to identify the β-sheet regions of Aβ fibrils.[5,6] Interestingly, the success of this method actually implies that proline can be incorporated into a β-sheet region because, as observed by Wetzel and co-workers, the validity of the method relies on the assumption that proline substitution would perturb but not destroy the β-sheet segment at the mutation site.[5] This assumption is partially justified by the fact that the morphology of amyloid fibrils formed by the proline mutants of $Aβ_{1–40}$ is very similar to that of wild-type fibrils. However, the question of why proline mutation would merely perturb the cross-β structure of the $Aβ_{1–40}$ fibrils and in some cases might even increase the number of hydrogen bonds remains unexplained.[5]

In the literature, a handful of proline-containing amyloid fibrils have been studied by solid-state NMR spectroscopy.[7–12] There is indeed some evidence showing that proline residues are, in general, not involved in the rigid core of

[a] N.-S. Lin, J. C.-H. Chao, H.-M. Cheng, F.-C. Chou, Dr. S.-J. Huang, Prof. J. C. C. Chan
Department of Chemistry
National Taiwan University
No. 1, Section 4, Roosevelt Road
Taipei 106 (Taiwan)
Fax: (+886) 2-23636359
E-mail: chanjcc@ntu.edu.tw

[b] Dr. C.-F. Chang, Dr. Y.-R. Chen, Dr. Y.-J. Chang
Genomics Research Center
Academia Sinica
Taipei (Taiwan)

Supporting information for this article is available on the WWW under http://dx.doi.org/10.1002/chem.200903290.

amyloid fibrils.[9,11] However, it has also been documented that the proline residues (P_{113}) of amyloid fibrils formed by the peptide fragment of transthyretin ($TTR_{105–115}$) have no substantial deviation from the β-strand conformation.[7,8] In a preliminary study of amyloid fibrils formed by the fragment of human prion protein ($huPrP_{23–144}$), the results of chemical shift analysis indicate that residue P_{137} is well incorporated into the β-strand region.[12] In spite of these observations, it remains surprising to find that the peptide fragment of $huPrP_{127–147}$, in which the proline residue P_{137} is located near the middle of the sequence, is amyloidogenic.[13] Therefore, $huPrP_{127–147}$ can serve as a useful model system to investigate the structural features of the amyloid fibrils formed by proline-containing sequences. Furthermore, it has been suggested that the tendency of $huPrP_{127–147}$ to form a twisted fibrillar structure might be associated with the morphology of the prion fibrils extracted from brains of humans with transmissible spongiform encephalopathies.[14] In fact, considerable efforts have been made to apply solid-state NMR spectroscopy to characterize the amyloid fibrils formed by different fragments of PrP, for example, Syrian hamster $PrP_{109–122}$,[15,16] mouse $PrP_{89–143}$,[10,17] $huPrP_{23–144}$,[12] and $huPrP_{106–126}$.[18]

Herein, we set out to characterize the molecular structure of the amyloid fibrils formed by $huPrP_{127–147}$ with the sequence Ac-GYMLGSAMSRPIIHFGSDYED-NH_2. We have developed a novel technique to identify solvent-protected backbone amide protons in an H/D exchange experiment without disaggregating the amyloid fibrils, from which we obtain strong evidence to prove that proline residue P_{137} does not disrupt the β-sheet structure from G_{127} to G_{142}. This somewhat counterintuitive result provides a rationalization for the proline mutagenesis approach at the molecular level. It may also serve as a benchmark for the structural study of the amyloid fibrils formed by other proline-containing fragments of human prion protein. Finally, we anticipate that the in situ detection of the H/D exchange process will find useful applications in the studies of other amyloid fibrils.

Results and Discussion

Fibril morphology: Transmission electron microscope (TEM) images of $huPrP_{127–147}$ fibrils incubated for 4 h and 12 d are shown in Figure 1. The 4 h sample mainly contains some short filaments (length $\leq$500 nm) and spherical aggregates of variable diameters ($\leq$50 nm). Because the 4 h sample does not exhibit any thioflavin T fluorescence (see Figure S1 of the Supporting Information), the spherical aggregates closely resemble the amylospheroids of β-amyloid.[19] In the 12 d sample, mature fibrils are found. Typically, a mature fibril has a width of approximately 15 nm, which is modulated periodically. Different fibrils have slightly different modulation periods, ranging from 80 to 120 nm. Our data confirm the earlier observation that $huPrP_{127–147}$ is amyloidogenic.[13] The morphology of the fibrils is indistinguishable from other amyloid fibrils. The incubation time required for the formation of $huPrP_{127–147}$ fibrils is comparable to that required for $A\beta_{1–40}$ fibrils.[20]

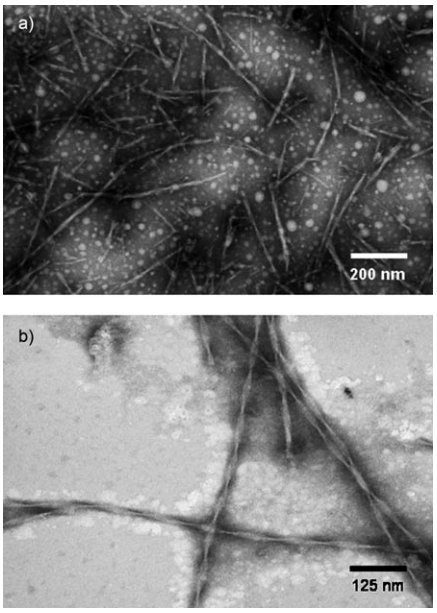

Figure 1. TEM images of the $huPrP_{127–147}$ fibrils with different incubation times; a) 4 h, b) 12 d.

Fibril cytotoxicity: The toxicity of our fibril samples on SH-SY5Y cells was examined by using a standard MTT assay as described in the Experimental Section. Figure 2 shows the neurotoxicity of the fibril samples at different concentrations and incubation times. In general, the cytotoxicity decreases with the peptide concentration. When the fibril concentration is reduced to 0.04 μM, the cytotoxicity is significantly lessened. It is worth noting that the cytotoxicities of the $huPrP_{127–147}$ fibrils formed at different incubation times are very similar. In particular, the cytotoxicity of the 0 d sample, in which the species of amylospheroids are expected to be very abundant, does not show any enhanced toxicity

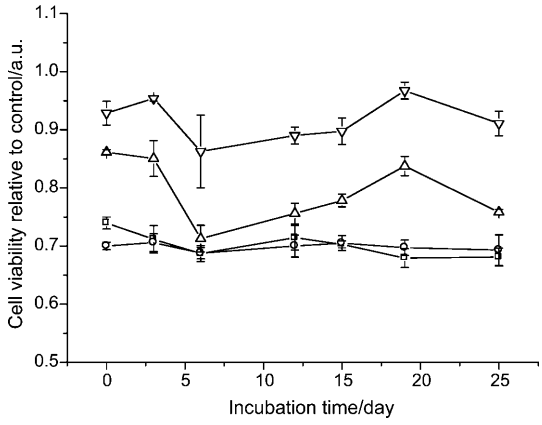

Figure 2. Cytotoxicity of the $huPrP_{127–147}$ fibrils as a function of the fibril concentration (□: 40 μM; ○: 4 μM; △: 0.4 μM; ▽: 0.04 μM) and incubation time.

compared with the samples containing mainly the mature fibrils. Apparently, the amylospheroids of huPrP$_{127–147}$ do not have higher cytotoxicity than the corresponding mature fibrils, in stark contrast to β-amyloid.[19,21]

^{13}C–^{13}C Chemical shift correlation data: Samples for solid-state NMR spectroscopic measurements were isotopically labeled at selected positions as summarized in Table 1. The

Table 1. Isotopic labeling of huPrP$_{127–147}$ fibril samples.

Sample	Labeling scheme
LASG	Uniform ^{15}N and ^{13}C labeling of L_{130}, A_{133}, S_{135}, G_{142}
GMSID	Uniform ^{15}N and ^{13}C labeling of G_{127}, M_{129}, S_{135}, I_{139}, D_{144}
ID	Uniform ^{15}N and ^{13}C labeling of I_{138}, D_{144}
MF	Uniform ^{15}N and ^{13}C labeling of M_{129}, F_{141}
PS	Uniform ^{15}N and ^{13}C labeling of P_{137}, S_{143}
L	^{13}C labeling of C′ at L_{130}
AG	^{13}C labeling of C_β at A_{133}, ^{13}C labeling of C′ at G_{142}

data of ^{13}C chemical shifts and linewidths were obtained from the two-dimensional ^{13}C–^{13}C chemical shift correlation spectra (see Table S1 of the Supporting Information). As an illustration, the spectrum measured for the PS sample is shown in Figure 3. The calculated secondary shifts are

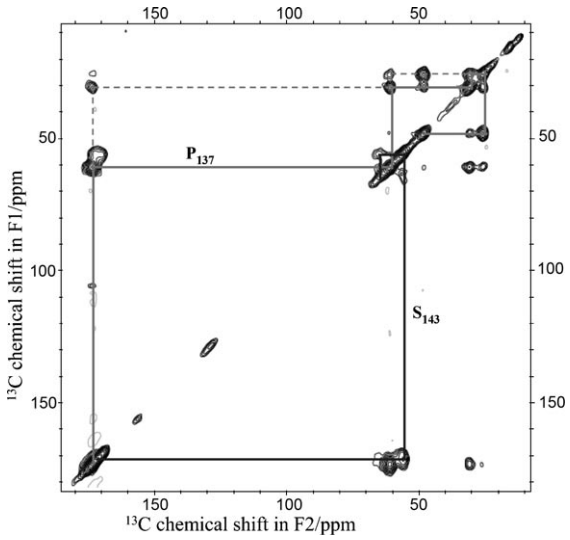

Figure 3. ^{13}C–^{13}C chemical shift correlation plot of the lyophilized PS sample. The dashed lines indicate relay polarization transfer.

shown in Figure 4, for which the random-coiled values were obtained from the literature.[22] The chemical shift data of the residues from G_{127} to G_{142} are consistent with a β-strand conformation.[22,23] For convenience, we refer to the β-strand region from G_{127} to R_{136} as β1, whereas the region from I_{138} to G_{142} is β2. The ^{13}C signals of D_{144} are so weak that it is difficult to determine the corresponding secondary shifts. Because the chemical shift difference between the C_β and C_γ of P_{137} is 5.2 ppm, we conclude that the R_{136} to P_{137} peptide

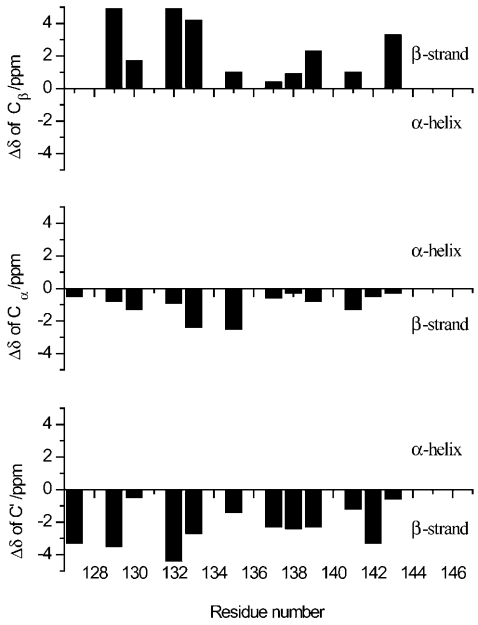

Figure 4. Secondary chemical shifts ($\Delta\delta$) calculated for selected residues of the fibril samples.

bond exists in a *trans* configuration.[7,11,24] This observation is consistent with the results of a molecular dynamics (MD) study of the K3 peptide that the *trans* configuration of the His–Pro linkage is more flexible than the *cis* configuration.[25]

On a millisecond time scale, dynamics of the fibrils will interfere with the transfer efficiency of the ^{1}H to ^{13}C cross-polarization. Therefore, the relative C′–C_α cross-peak intensities, which can also depend on the ^{13}C–^{13}C transfer efficiency and relaxation behaviors, can be used to probe for the presence of structural dynamics in a qualitative way. With reference to Figure 5a, the largest peak intensity at P_{137} is consistent with the expected structural rigidity of P_{137}. The peak intensities of the residues near the C terminus are relatively low, revealing the substantial structural dynamics there. In comparison, our data show that the residues near the N terminus are less mobile. Based on the full widths at half maximum ($\Delta\nu_{1/2}$) of the ^{13}C signals at the labeled sites (see Figure 5b), the highest structural order is found near the middle of β1, whereas the region near P_{137} has somewhat larger structural heterogeneity. The $\Delta\nu_{1/2}$ data near the C terminus are significantly larger than the average value. We believe that the presence of substantial structural heterogeneity near the C terminus is a direct consequence of the structural dynamics. The chemical shift analysis discussed above indicates that the β-strand structure of huPrP$_{127–147}$ extends from G_{127} to G_{142}. In particular, the ^{13}C chemical shift data determined for P_{137} ($\delta = 173.3$ (C′), 61.0 (C_α), 31.0 (C_β), 25.8 (C_γ), 48.4 (C_δ), and 134.8 ppm (CN_H)) are quite similar to those reported for P_{113} in TTR$_{105–115}$ ($\delta = 174.8$ (C′), 62.6 (C_α), 32.6 (C_β), 28.0 (C_γ), 49.6 (C_δ), and 135.8 ppm (CN_H)), which has no substantial deviation from the β-sheet structure.[7] By using TALOS,[26] which is well established for the

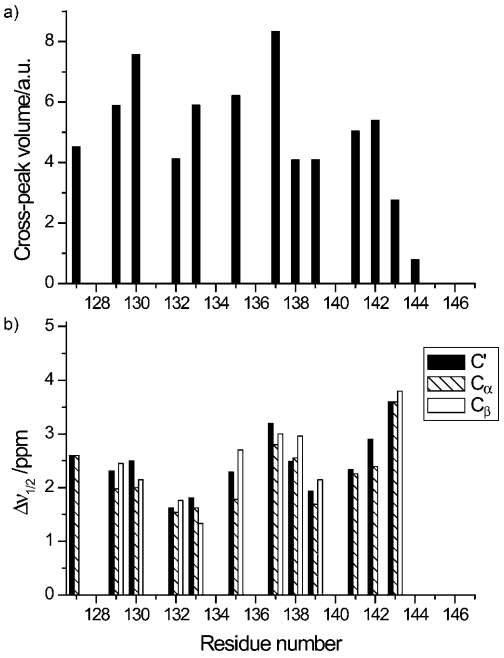

Figure 5. Intensity and linewidth data obtained from the ^{13}C–^{13}C correlation spectra of uniformly labeled samples. a) Relative signal intensities of the cross-peaks of C′ and C_α. b) Full widths at half maximum of the C′, C_α, and C_β signals.

structural determination of amyloid fibrils, the chemical shift data were employed to predict the backbone torsion angles of the huPrP$_{127–147}$ fibrils (see Table 2). Again, the data support the observation that the β-strand conformation is not disrupted in the region of P_{137}.

Table 2. Backbone torsion angles predicted for selected residues of huPrP$_{127–147}$ by using TALOS.

Residue	ϕ [°]	ψ [°]
M_{129}	−141±14	149±13
L_{130}	−113±19	128±13
G_{131}	−141±16	151±13
S_{132}	−142±15	154±15
A_{133}	−142±16	151±13
R_{136}	−177±24	129±14
P_{137}	−78±26	139±14
I_{138}	−118±24	129±14
I_{139}	−118±7	130±15
S_{143}	−136±15	148±13

Distance measurement between neighboring peptides: To probe the internuclear distance between the ^{13}C nuclei in close proximity, we employed the ^{13}C constant-time finite-pulse radio-frequency-driven recoupling (fpRFDR-CT) technique,[27] which has been successfully applied to the studies of amyloid fibrils.[16,20] For the study of huPrP$_{127–147}$ fibrils, we prepared samples AG and L. The AG sample is labeled with $^{13}C_\beta$ at A_{133} and $^{13}C'$ at G_{142}, whereas the L sample is labeled with $^{13}C'$ at L_{130}. To quantify the spacing between the β-strands (*d*), the fpRFDR-CT data were compared with simulations on a linear chain of six spins with *d* varied from 4 to 7 Å (see Figure 6). The contribution from

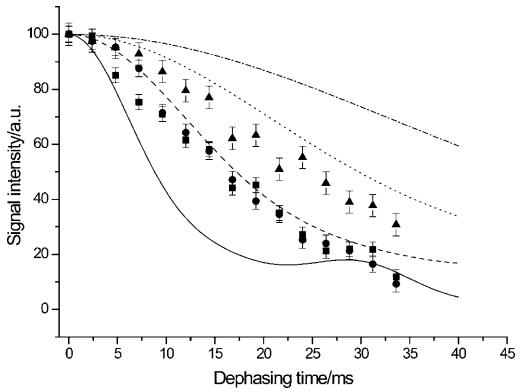

Figure 6. ^{13}C fpRFDR-CT spectroscopy data of the samples with ^{13}C labeling at selected positions (■: C′ at G_{142}; ●: C_β at A_{133}; ▲: C′ at L_{130}). The lines are simulations on a linear array of six spins at different nearest-neighbor distances (——: 4; -----: 5; •••••: 6; –•–•: 7 Å).

the natural abundance signals were corrected for by using the procedure described in the literature.[20] From the corresponding χ^2 plot, the *d* values at A_{133} and G_{142} were both determined to be (4.9±0.2) Å at 90% confidence level. The corresponding *d* value at L_{130} is found to be (5.6±0.3) Å. Because the A_{133} residue is labeled at C_β, shifting the hydrogen bond registry away from in-register alignment by one residue in either direction will increase the *d* value to approximately 7 Å. Therefore, our results provide unequivocal evidence that the organization of the β strands is in-register parallel.

After we incorporate all the structural constraints obtained thus far for the huPrP$_{127–147}$ fibrils, the intriguing effect of P_{137} on the fibril structure becomes apparent. Because of the kink due to the *trans* configuration of the R_{136}–P_{137} linkage, it is impossible to adopt a perfect cross-β structural motif for both the β1 and β2 regions simultaneously. As illustrated in Figure 7, if the β1 region is aligned

Figure 7. Schematic representation of the in-register parallel β sheet formed by huPrP$_{127–147}$. This cartoon highlights the kink at P_{137} that prevents the formation of simultaneous idealized cross-β structures at the β1 and β2 regions. Here, we arbitrarily align the β1 region to form an idealized cross-β structure.

to adopt a perfect cross-β structure it is impossible to form intermolecular hydrogen bonding in the β2 region, and vice versa. Thus, it is very interesting to determine which region, β1 or β2, would preferentially form a cross-β structure. One possible method to address this question is to probe for the hydrogen bonding in the β1 and β2 regions by H/D exchange experiments.

H/D exchange: H/D exchange experiments can be used to identify solvent-protected backbone amide protons in amyloid fibrils. In brief, the amyloid fibrils are first incubated in deuterated buffer. After quenching the H/D exchange, the fibrils must be disaggregated into monomers. The residues at which the amide protons are exchanged to deuterons can then be detected by mass spectrometry[28] or solution-state NMR spectroscopy.[29] Herein, we suggest that the dissolution of the amyloid fibrils is not necessary if solid-state NMR spectroscopy is used as the detection method. Under the high-resolution conditions provided by magic-angle spinning, the technique of $^{15}N\{^1H\}$ cross-polarization (CP) can be used to select the signals of nitrogen atoms that are in close proximity to protons. In particular, when the CP contact time is set to 100 μs, the ^{15}N signals of the deuterated amide groups would be largely suppressed. By using this simple strategy, the in situ characterization of H/D exchange in amyloid fibrils could be realized.

As a proof-of-principle experiment, we measured the $^{15}N\{^1H\}$ CP spectra of our PS sample, which is the fibril sample with uniform ^{15}N and ^{13}C labeling at P_{137} and S_{143}. Figure 8 shows the spectra of the PS sample (without any H/D exchange) obtained at two contact times, 2 ms and 100 μs. For the 2 ms spectrum, two amide nitrogen signals are observed, in which the peaks at $\delta = 135$ and 117 ppm are assigned to the amide nitrogen of P_{137} and S_{143}, respectively.[7] When the CP contact time is reduced to 100 μs, the $^{15}N\{^1H\}$ CP signal would be dominated by the one-bond ^1H–^{15}N transfer, which is referred to as the $^{15}N_H$ signal in the subsequent discussion. Accordingly, the $^{15}N_H$ signal of P_{137} is not detectable because proline does not have an amide proton. As expected, the $^{15}N_H$ signal of S_{143} is still observable under the same experimental conditions, and has approximately the same intensity as the 2 ms $^{15}N\{^1H\}$ signal. Therefore, it is plausible to monitor the H/D exchange of amide protons by measuring the corresponding $^{15}N_H$ signals without disassembling the fibrils into monomers.

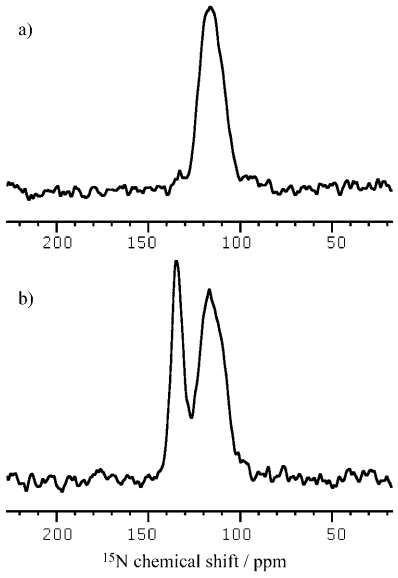

Figure 8. $^{15}N\{^1H\}$ CPMAS spectra of the PS sample at a spinning frequency of 20 kHz. a) Contact time of 100 μs, b) contact time of 2 ms.

We first define the protection factor of the amide proton as the ratio of the $^{15}N_H$ signal intensities of the sample with and without H/D exchange. After 42 h of H/D exchange, the protection factors were found to be 0.07 ± 0.03 and 0.6 ± 0.3 for S_{143} and I_{138}, respectively. The relatively large errors are mainly due to the uncertainty in the amount of salts left in the samples. To alleviate this problem, we redefined the protection factor as the ratio of the signal intensities of $^{15}N_H$ and ^{15}N with the contact time of the corresponding $^{15}N\{^1H\}$ CP experiments set to 100 μs and 2 ms, respectively. The obtained protection factor for I_{138} is 0.65 ± 0.1. The error bar here was determined by the root-mean-square noise of the spectrum. This modified strategy was then applied to the measurements of the LASG and GMSID samples. The results shown in Figure 9 are completely in line with the chemical shift data that shows that the β-strand structure of $huPrP_{127–147}$ extends from G_{127} to G_{142}. More importantly, our H/D exchange experiments qualitatively prove that the backbone amide protons of the β1 and β2 regions are both involved in intermolecular hydrogen bonding. Thus, the only structural scenario consistent with the H/D exchange data is that each peptide strand of the $huPrP_{127–147}$ fibrils must have a twist about the fibril axis, pivoting on P_{137}, so that the neighboring peptide strands could form hydrogen bonds to a certain extent in both the β1 and β2 re-

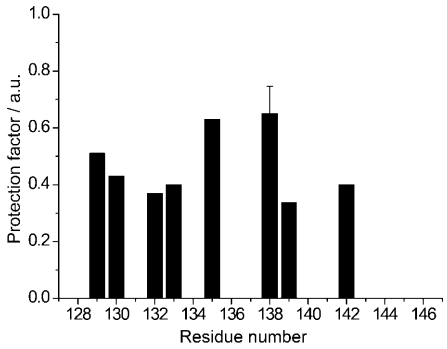

Figure 9. Protection factors of the amide protons. The protection factors were obtained by taking the ratio of the $^{15}N_H$ signals to the ^{15}N signals, which were obtained by $^{15}N\{^1H\}$ CPMAS spectroscopy with contact times of 100 μs and 2 ms, respectively. The error bar was determined from the root-mean-square noise of the signal-free region.

gions. For this twisted cross-β structure, the hydrogen bonds linking two adjacent β-strands would not be parallel to the fibril long axis.

Structural model of huPrP$_{127–147}$ fibrils: An initial structural model for the huPrP$_{127–147}$ fibril was constructed by arranging 16 peptide strands into a parallel in-register β sheet. To maintain the intermolecular hydrogen bonding to a reasonable extent in both the β1 and β2 regions, each β strand was arbitrarily twisted by 2.8° about the fibril long axis pivoted on P_{137}. The interstrand distance measured at P_{137} was set to 6 Å. The restrained energy minimization was then carried out to optimize the initial structure as described in the Supporting Information. Figure 10 shows the preliminary structural model of the huPrP$_{127–147}$ fibrils after energy minimization. The hydrogen-bonding networks in the β1 and β2 regions have been verified by HBPLUS (version 3.15;[30] see Table S2 in the Supporting Information). The twist angle and the interstrand distance were reduced to (2.4 ± 0.3)° and (5.5 ± 0.1) Å, respectively, in which the standard deviations were obtained by analyzing each adjacent pair of the β strands.

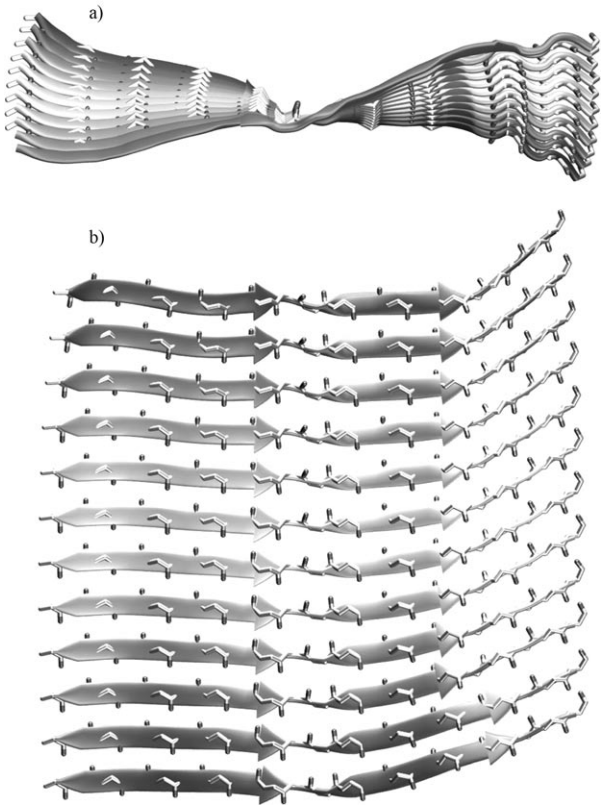

Figure 10. Structural model of the huPrP$_{127–147}$ fibrils obtained from the restrained energy minimization. The twist between adjacent peptide strands is a compromise that maintains sufficient hydrogen bonding in both the β1 and β2 regions. Only the central 12 peptide strands of our model are shown. a) Viewed parallel to the fibril long axis, b) viewed perpendicular to the fibril long axis. A color version of this figure is shown in the Supporting Information.

It is worth noting that the model shown in Figure 10 merely depicts the local structure of a single cross-β unit of the huPrP$_{127–147}$ fibrils. It does not imply that all the side-chains are exposed to the solvent or that the protofilament contains a single cross-β unit only. Furthermore, the TEM data show that the fibril width is about 15 nm, which suggests that the protofilament should comprise more than a single extended β strand. Thus, our structural model requires further experimental corroboration, such as the characterization of the quaternary contacts. Nevertheless, it is firmly established experimentally that a proline residue could well be incorporated into the cross-β structure of amyloid fibrils, which explains why a proline mutation would merely perturb the cross-β structure of the Aβ$_{1–40}$ fibrils or even increase the extent of hydrogen bonding.[5] Recently, proline mutagenesis has been successfully employed to establish the correlation of the β-sheet segment and the infectivity of HET-s fibrils.[34] In most cases, proline substitution in β-strand regions would disrupt the β-sheet structure, and subsequently lead to a loss of the infectivity. Interestingly, it has also been observed that a number of proline substitutions in β-strand regions interfered only partially with amyloid formation. This observation implies that certain β-strand regions of HET-s are flexible enough to incorporate the kink formed at the proline substitution site, without disrupting the β-strand conformation. Very recently, the rat- and human-islet amyloid polypeptide (IAPP) have been extensively studied to unravel the origin of their different toxicities to β-cell membrane.[35–37] The rat-IAPP differs from the human-IAPP by six residues; the rat-IAPP sequence has three proline residues at P25, P28, and P29, whereas human-IAPP does not have any proline residues. The fact that rat-IAPP is nonamyloidogenic is consistent with our data: Because of the kink formation at the proline site, the presence of three proline residues in close vicinity represents a very effective disrupter of β-sheet structure.

Periodically twisted morphology is commonly observed in amyloid fibrils. In fact, the twisted and untwisted Aβ$_{1–40}$ fibrils obtained under different incubation conditions have different underlying molecular structures.[31] To date, the physical origin for the appearance of twisted morphology is largely unknown. A recent molecular dynamics simulation suggests that there is no single dominant term that accounts for the degree of twist in the amyloid fibrils formed by GNNQQNY.[32] Very recently, Paravastua et al. demonstrated that the twisted structure observed for Aβ$_{1–40}$ fibrils can be accounted for by the presence of a three-fold symmetry about the fibril growth axis.[33] The twisted morphology of the huPrP$_{127–147}$ fibrils, on the other hand, might be correlated to the kink produced at P_{137}, which generates a twist between adjacent peptide strands to maintain hydrogen bonding in the β1 and β2 regions. However, additional work, such as molecular dynamics simulations, is required to clarify this issue.

Conclusion

For the huPrP$_{127–147}$ fibrils, the chemical shift data indicate that there is no substantial distortion of the backbone torsion angles away from the β-strand region. Although further direct measurements of the backbone torsion angles in the region of P$_{137}$ are required to refine the structural model shown in Figure 10, the in-register parallel structure and the presence of intermolecular hydrogen bonding in both the β1 and β2 regions are firmly supported by our NMR spectroscopy data. The method of proline mutagenesis has been successfully used to identify β-sheet regions of amyloid fibrils as documented in the literature.[5,6] Wetzel and co-workers have systematically characterized the kinetic and thermodynamic aspects of the method.[5] We believe our findings have, on the other hand, clarified the structural basis of the proline mutagenesis method. When proline replaces a residue of the β-strand, the kink formed at the position of the proline residue will considerably weaken the hydrogen bonding between the neighboring strands, especially when the mutation site is near the central region of a β sheet. This effect will be less prominent in the non-β-sheet region.

H/D exchange experiments have been established as a useful technique to identify the amyloid core of an amyloidogenic peptide or protein. The most challenging step of the conventional H/D exchange experiment is the rapid conversion of the fibrils into the corresponding monomers for subsequent detection. Although [D$_6$]DMSO is a reliable solvent for the dissolution of amyloid fibrils, it is not trivial to minimize the effect of backward exchange.[29] Different solvent mixtures have been suggested for different amyloid systems, showing that it is largely an empirical task to prepare the quenching buffer for an H/D exchange experiment.[38] Herein, we demonstrate that solid-state NMR spectroscopy allows an in situ detection of the H/D exchange process without disturbing the fibrillar state of interest. Our method is so straightforward that it can be readily implemented for the measurement of any fibril systems that are uniformly labeled by ^{13}C and ^{15}N isotopes. The idea can be easily extended to incorporate any progress in the resolution enhancement of biological solid-state NMR spectroscopy.

Experimental Section

Sample preparation: All the chemicals were obtained from NovaBiochem unless stated otherwise. HuPrP$_{127–147}$ peptides (sequence Ac-GYMLGSAMSRPIIHFGSDYED-NH$_2$) were synthesized by using an automated Odyssey microwave peptide synthesizer (CEM, Matthews, USA). Peptide purity was at least 90% as determined by MALDI-TOF mass spectrometry. The yield of purified peptide was approximately 23%. ^{13}C- and ^{15}N-labeled amino acids with FMOC protection were obtained from Cambridge Isotope Laboratories (Andover, USA), CortecNet (Tilleuls, France), and Isotec (St. Louis, USA). Fibril samples were formed by dissolving the purified peptides in phosphate buffer (10 mM; concentration of NaCl was increased to 396 mM) with addition of NaN_3 (0.01%). The peptide concentration was set to 400 μM. After sonication (6 W) in ice bath for 5 min, the sample was incubated at 37 °C for 12 d.

Cytotoxicity assay: The MTT (3-(4,5-dimethylythiazol-2-yl)-2,5-diphenyltetrazolium bromide) assay was used to perform cytotoxicity test on our fibril samples. A number of 2×10^4 human neuroblastoma SH-SY5Y cells per well were seeded in a 96-well plate (Corning). The cells were incubated at 37 °C under a humidified 5% CO_2 atmosphere for 24 h in phenol red-free Dulbecco's modified Eagle medium (DMEM)/F12 (100 μL; Gibco) with 10% fetal bovine serum (Gibco) and 1% penicillin/streptomycin (Gibco). Fibril samples were serially diluted into different concentrations by the incubation buffer. An aliquot (10 μL) of the fibril sample was added to the cells in each well. After incubating for 24 h in the growth chamber, the MTT solution (10 μL; 5 mg mL^{-1} in DMEM/F12) was added into each well. After 3 h, a warm lysis buffer containing isopropanol with 0.1 N HCl was added to each well. Absorbance at $\lambda=570$ and 690 nm were measured by using an ELISA reader (Molecular Devices Corporation, Sunnyvale, USA). Data were processed to obtain the absorbance difference of $\lambda=570$ and 690 nm for an average of five measurements. Each data set was normalized by using negative controls.

Transmission electron microscopy: An aliquot (10 μL) of fibril sample was suspended on a carbon-coated copper grid for 1 min. Aliquots (10 μL) of deionized H_2O were added and blotted three times to remove the salt. After staining with 2% phosphotungstic acid (PTA) for 1 min, TEM images were recorded by using a Hitachi H-7100 electron microscope operated at 80 kV.

Solid-state NMR spectroscopy: The salts of the fibril samples were first removed by dialysis for 17 h (Cellu Sep H1 part #0550-40 MWCO: 5000) and then lyophilized. All NMR spectroscopy experiments were carried out at frequencies of 75.5 and 300.1 MHz for ^{13}C and ^{1}H, respectively, by using a Bruker DSX300 NMR spectrometer equipped with a commercial 2.5 mm triple-resonance probe. ^{13}C NMR chemical shifts were referenced to TMS with adamantane as the secondary reference standard. ^{13}C–^{13}C chemical shift correlation spectra were measured at an MAS frequency of 25.0 kHz based on the finite-pulse radio-frequency-driven recoupling (fpRFDR) technique.[39] Continuous-wave and XiX[40] proton decouplings of 100 kHz were applied during recoupling periods and the t_2 acquisition, respectively. Chemical shift and linewidth data were obtained by fitting each cross peak to a Gaussian by using the package NMRPipe.[41] The ^{13}C–^{15}N chemical shift correlation spectra were measured at a spinning frequency of 10 kHz by using the double cross-polarization technique with a mixing time of 4 ms.[42] ^{15}N NMR chemical shifts were referenced to liquid NH_3 by indirect referencing.[43] ^{13}C–^{13}C dipolar recoupling measurements were carried out with the fpRFDR-CT technique,[27,39] at an MAS frequency of 20.0 kHz. During the fpRFDR recoupling periods, the ^{13}C π pulses were set to 15 μs. The ^{13}C π/2 pulses flanking the fpRFDR pulse blocks were set to 4 μs.[27] Numerical analysis of the fpRFDR-CT data were carried out by using the package SIMPSON[44] (version 1.1.0) and SPINEVOLUTION[45] (version 3.0) as described earlier.[16]

H/D exchange: The isotopically labeled fibril samples selected for H/D exchange studies were prepared as described above. The fibrils in the buffer solution were collected by centrifugation, suspended in freshly obtained D_2O, and shaken at 250 rpm under N_2 atmosphere for 42 h. The samples were then lyophilized to quench the H/D exchange. The dried samples were packed in a rotor for subsequent ^{15}N{^{1}H} CPMAS measurements.

Molecular modeling: An initial structural model consisting of 16 strands was constructed as a parallel in-register β sheet by Discovery Studio Visualizer 2.0 (Accelrys). The backbone torsion angles (ϕ/ψ) of all the residues were set to their idealized values, that is, −60/140° for Pro, and −140/140° otherwise. The twist angle of two adjacent strands and the interstrand distance were arbitrarily set to 2.8° and 6 Å, respectively. After that, restrained energy minimization was carried out by using the program TINKER (version 4.2). All atoms of the system were considered explicitly, and their interactions were calculated by using the Amber99 force field.[46] The model shown in Figure 10 was created by VMD (version 1.8.6).[47]

Acknowledgements

This work was supported by grants from the National Science Council and the Ministry of Education. We thank Shin-Wen Lee for her valuable suggestions at the early stage of this work.

[1] F. Chiti, C. M. Dobson, *Annu. Rev. Biochem.* **2006**, *75*, 333–366.
[2] C. M. Dobson, *Nature* **2003**, *426*, 884–890.
[3] R. Tycko, *Q. Rev. Biophys.* **2006**, *39*, 1–55; A. Naito, I. Kawamura, *Biochim. Biophys. Acta Biomembr.* **2007**, *1768*, 1900–1912; H. Heise, *ChemBioChem* **2007**, *8*, 179–189.
[4] A. K. Thakur, R. Wetzel, *Proc. Natl. Acad. Sci. USA* **2002**, *99*, 17014–17019; W. C. Wigley, M. J. Corboy, T. D. Cutler, P. H. Thibodeau, J. Oldan, M. G. Lee, J. Rizo, J. F. Hunt, P. J. Thomas, *Nat. Struct. Biol.* **2002**, *9*, 381–388.
[5] A. D. Williams, E. Portelius, I. Kheterpal, J. T. Guo, K. D. Cook, Y. Xu, R. Wetzel, *J. Mol. Biol.* **2004**, *335*, 833–842.
[6] D. F. Moriarty, D. P. Raleigh, *Biochemistry* **1999**, *38*, 1811–1818; S. J. Wood, R. Wetzel, J. D. Martin, M. R. Hurle, *Biochemistry* **1995**, *34*, 724–730; A. Morimoto, K. Irie, K. Murakami, H. Ohigashi, M. Shindo, M. Nagao, T. Shimizu, T. Shirasawa, *Biochem. Biophys. Res. Commun.* **2002**, *295*, 306–311.
[7] C. P. Jaroniec, C. E. MacPhee, N. S. Astrof, C. M. Dobson, R. G. Griffin, *Proc. Natl. Acad. Sci. USA* **2002**, *99*, 16748–16753.
[8] C. P. Jaroniec, C. E. MacPhee, V. S. Bajaj, M. T. McMahon, C. M. Dobson, R. G. Griffin, *Proc. Natl. Acad. Sci. USA* **2004**, *101*, 711–716.
[9] H. Heise, W. Hoyer, S. Becker, O. C. Andronesi, D. Riedel, M. Baldus, *Proc. Natl. Acad. Sci. USA* **2005**, *102*, 15871–15876; H. Heise, M. S. Celej, S. Becker, D. Riede, A. Pelah, A. Kumar, T. M. Jovin, M. Baldus, *J. Mol. Biol.* **2008**, *380*, 444–450; M. Vilar, H. T. Chou, T. Luhrs, S. K. Maji, D. Riek-Loher, R. Verel, G. Manning, H. Stahlberg, R. Riek, *Proc. Natl. Acad. Sci. USA* **2008**, *105*, 8637–8642; R. B. Wickner, F. Dyda, R. Tycko, *Proc. Natl. Acad. Sci. USA* **2008**, *105*, 2403–2408.
[10] K. Hun Lim, T. N. Nguyen, S. M. Damo, T. Mazur, H. L. Ball, S. B. Prusiner, A. Pines, D. E. Wemmer, *Solid State Nucl. Magn. Reson.* **2006**, *29*, 183–190.
[11] K. Iwata, T. Fujiwara, Y. Matsuki, H. Akutsu, S. Takahashi, H. Naiki, Y. Goto, *Proc. Natl. Acad. Sci. USA* **2006**, *103*, 18119–18124.
[12] J. J. Helmus, K. Surewicz, P. S. Nadaud, W. K. Surewicz, C. P. Jaroniec, *Proc. Natl. Acad. Sci. USA* **2008**, *105*, 6284–6289.
[13] G. Forloni, N. Angeretti, R. Chiesa, E. Monzani, M. Salmona, O. Bugiani, F. Tagliavini, *Nature* **1993**, *362*, 543–546.
[14] F. Tagliavini, F. Prelli, L. Verga, G. Giaccone, R. Sarma, P. Gorevic, B. Ghetti, F. Passerini, E. Ghibaudi, G. Forloni, M. Salmona, O. Bugiani, B. Frangione, *Proc. Natl. Acad. Sci. USA* **1993**, *90*, 9678–9682.
[15] J. Heller, A. C. Kolbert, R. Larsen, M. Ernst, T. Bekker, M. Baldwin, S. B. Prusiner, A. Pines, D. E. Wemmer, *Protein Sci.* **1996**, *5*, 1655–1661.
[16] S. W. Lee, Y. Mou, S.-Y. Lin, F.-C. Chou, W.-H. Tseng, C.-H. Chen, C.-Y. D. Lu, S. S.-F. Yu, J. C. C. Chan, *J. Mol. Biol.* **2008**, *378*, 1142–1154.
[17] D. D. Laws, H. M. L. Bitter, K. Liu, H. L. Ball, K. Kaneko, H. Wille, F. E. Cohen, S. B. Prusiner, A. Pines, D. E. Wemmer, *Proc. Natl. Acad. Sci. USA* **2001**, *98*, 11686–11690.
[18] P. Walsh, K. Simonetti, S. Sharpel, *Structure* **2009**, *17*, 417–426.
[19] M. Hoshi, M. Sato, S. Matsumoto, A. Noguchi, K. Yasutake, N. Yoshida, K. Sato, *Proc. Natl. Acad. Sci. USA* **2003**, *100*, 6370–6375.
[20] J. J. Balbach, A. T. Petkova, N. A. Oyler, O. N. Antzutkin, D. J. Gordon, S. C. Meredith, R. Tycko, *Biophys. J.* **2002**, *83*, 1205–1216.
[21] S. Chimon, M. A. Shaibat, C. R. Jones, D. C. Calero, B. Aizezi, Y. Ishii, *Nat. Struct. Mol. Biol.* **2007**, *14*, 1157–1164.
[22] D. S. Wishart, C. G. Bigam, A. Holm, R. S. Hodges, B. D. Sykes, *J. Biomol. NMR* **1995**, *5*, 67–81.
[23] D. S. Wishart, B. D. Sykes, *J. Biomol. NMR* **1994**, *4*, 171–180.
[24] S. K. Sarkar, D. A. Torchia, K. D. Kopple, D. L. VanderHart, *J. Am. Chem. Soc.* **1984**, *106*, 3328–3331.
[25] C. Liang, P. Derreumaux, N. Mousseau, G. Wei, *Biophys. J.* **2008**, *95*, 510–517.
[26] G. Cornilescu, F. Delaglio, A. Bax, *J. Biomol. NMR* **1999**, *13*, 289–302.
[27] Y. Ishii, J. J. Balbach, R. Tycko, *Chem. Phys.* **2001**, *266*, 231–236.
[28] I. Kheterpal, R. Wetzel, *Acc. Chem. Res.* **2006**, *39*, 584–593.
[29] M. Hoshino, H. Katou, K. Yamaguchi, Y. Goto, *Biochim. Biophys. Acta Biomembr.* **2007**, *1768*, 1886–1899.
[30] I. K. McDonald, J. M. Thornton, *J. Mol. Biol.* **1994**, *238*, 777–793.
[31] A. T. Petkova, R. D. Leapman, Z. H. Guo, W. M. Yau, M. P. Mattson, R. Tycko, *Science* **2005**, *307*, 262–265.
[32] X. Periole, A. Rampioni, M. Vendruscolo, A. E. Maro, *J. Phys. Chem. B* **2009**, *113*, 1728–1737.
[33] A. K. Paravastua, R. D. Leapman, W. M. Yau, R. Tycko, *Proc. Natl. Acad. Sci. USA* **2008**, *105*, 18349–18354.
[34] C. Ritter, M. L. Maddelein, A. B. Siemer, T. Luhrs, M. Ernst, B. H. Meier, S. J. Saupe, R. Riek, *Nature* **2005**, *435*, 844–848.
[35] J. R. Brender, U. H. N. Durr, D. Heyl, M. B. Budarapu, A. Ramamoorthy, *Biochim. Biophys. Acta Rev. Biomembr.* **2007**, *1768*, 2026–2029.
[36] P. E. S. Smith, J. R. Brender, A. Ramamoorthy, *J. Am. Chem. Soc.* **2009**, *131*, 4470–4478.
[37] R. Soong, J. R. Brender, P. M. Macdonald, A. Ramamoorthy, *J. Am. Chem. Soc.* **2009**, *131*, 7079–7085.
[38] A. S. P. Svane, K. Jahn, T. Deva, A. Malmendal, D. E. Otzen, J. Dittmer, N. C. Nielsen, *Biophys. J.* **2008**, *95*, 366–377.
[39] Y. Ishii, *J. Chem. Phys.* **2001**, *114*, 8473–8483.
[40] A. Detken, E. H. Hardy, M. Ernst, B. H. Meier, *Chem. Phys. Lett.* **2002**, *356*, 298–304.
[41] F. Delaglio, S. Grzesiek, G. W. Vuister, G. Zhu, J. Pfeifer, A. Bax, *J. Biomol. NMR* **1995**, *6*, 277–293.
[42] M. Baldus, A. T. Petkova, J. Herzfeld, R. G. Griffin, *Mol. Phys.* **1998**, *95*, 1197–1207; J. H. Yang, F. C. Chou, D. L. M. Tzou, *J. Magn. Reson.* **2008**, *195*, 116–120.
[43] D. S. Wishart, C. G. Bigam, J. Yao, F. Abildgaard, H. J. Dyson, E. Oldfield, J. L. Markley, B. D. Sykes, *J. Biomol. NMR* **1995**, *6*, 135–140.
[44] M. Bak, J. T. Rasmussen, N. C. Nielsen, *J. Magn. Reson.* **2000**, *147*, 296–330.
[45] M. Veshtort, R. G. Griffin, *J. Magn. Reson.* **2006**, *178*, 248–282.
[46] W. D. Cornell, P. Cieplak, C. I. Bayly, I. R. Gould, K. M. Merz, D. M. Ferguson, D. C. Spellmeyer, T. Fox, J. W. Caldwell, P. A. Kollman, *J. Am. Chem. Soc.* **1995**, *117*, 5179–5197.
[47] W. Humphrey, A. Dalke, K. Schulten, *J. Mol. Graph.* **1996**, *14*, 33–38.

Received: December 1, 2009
Published online: March 31, 2010

